Electrospray Plume Evolution Via Discrete Simulations

McKenna J. Davis[1], Adam L. Collins[2], Richard E. Wirz[3]
University of California, Los Angeles, CA, 90095, USA

The University of California, Los Angeles (UCLA) Plasma & Space Propulsion Laboratory (PSPL) has developed an Interaction Model which simulates electrospray droplet dynamics immediately following emission through expansion into a plume. Simulation results offer insight into plume expansion as the culmination of fundamental physics governing charged droplet motion. This publication emphasizes the role of velocity differences between droplets in provoking clustering events with resulting large-magnitude Coulombic interactions that facilitate plume expansion. Simulated plume profiles show the propensity of smaller, high-specific charge droplets to occupy wide plume angles, and heavier, low-specific-charge droplets to remain near the axis of emission. Plume profile results demonstrate a high sensitivity to the modal distribution of the droplet population, motivating further research on droplet emission and breakup processes.

I. Nomenclature

d	=	emitter-separation distance
I	=	emitter current
m	=	mass
q	=	charge
r	=	radius
Q	=	volumetric flow rate
V	=	emitter bias voltage
$\dot{m}$	=	mass flux
t	=	time
F_E	=	electrostatic force
ρ_e	=	charge density
ε	=	permittivity
ρ	=	density
γ	=	surface tension
σ	=	conductivity
E	=	electric field magnitude
ϕ	=	electric potential
F_d	=	total force on droplet
k	=	Coulomb constant
U	=	velocity of fluid medium
v_d	=	droplet velocity
g	=	acceleration rate due to gravity
Δt	=	computational time step
τ	=	dimensionless time
T_P	=	period of perturbation
C_D	=	coefficient of drag
Re	=	Reynold's number
z	=	percent of distance from emitter to extractor grid
N	=	number of droplets in simulation
θ	=	polar half-angle w.r.t beam ax

[1] Graduate Student, Department of Mechanical & Aerospace Engineering, mjdavis325@g.ucla.edu.
[2] Research Scientist, Department of Mechanical & Aerospace Engineering, collinsalc55@ucla.edu.
[3] Professor, Department of Mechanical & Aerospace Engineering, wirz@ucla.edu.

II. Introduction

Electrospray thrusters are a highly scalable form of electric propulsion with a wide range of specific impulse capabilities. In 2015, such thrusters first demonstrated in-space operation with the Colloid MicroNewton Thruster (CMNT), developed by Busek Co., Inc and NASA Jet Propulsion Laboratory (JPL) for the European Space Agency (ESA) Laser Interferometer Space Antenna (LISA) Pathfinder mission [1]. The CMNT demonstrated micronewton thrust precision and low thrust-noise capabilities (100 nN/$Hz^{1/2}$), with seven of the eight CMNT thrusters operating for over 2,400 hours. The ESA LISA mission requires up to 60,000 hours of operational lifetime; therefore, understanding life-limiting mechanisms in electrospray thrusters is an indispensable effort in improving their viability for this and other future missions [2].

Electrospray thrusters have a variety of failure modes outlined in the UCLA Plasma and Space Propulsion Laboratory (PSPL) [3]Electrospray Life Model [4], [5]. The primary threat to thruster life is propellant overspray to the extractor and accelerator grids. Propellant overspray involves droplets at sufficiently wide plume angles impinging on porous downstream grids until they are sufficiently saturated, at which point propellant may spray back to an upstream grid or the emitter. Failure via propellant back-spray is provoked by mass flux to the grids; thus, the frequency of grid impingement and mass of impinging droplets are key parameters in thruster lifetime estimation. Predicting droplet mass and impingement frequency requires a rigorous study of droplet dynamics throughout the droplet's lifetime in the thruster: from emission, through electrostatic acceleration and Coulombic interactions in the plume, to thrust production or grid impingement. The UCLA PSPL utilizes experimentation and computational modeling synergistically to research plume evolution; experiments motivate and validate simulation results while computational models illuminate underlying electrospray physics [2], [6], [7]. Computational models possess many characteristics highly suitable for predictions pertaining to thruster life. Large numbers of potential thruster designs can be tested with greater ease and efficiency computationally than experimentally. Additionally, gravity, drag, and other potential facility effects can be neglected easily in a simulation. Furthermore, computational models can observe droplet properties and trajectories at any point in the simulation domain without influencing droplet dynamics.

The UCLA PSPL has conceptually discretized the cone-jet mode electrospray into intersecting regimes for discussion and computational modeling purposes (Figure 1) [2]. In the Extraction Region, the axisymmetric cone-jet forms and emits droplets. The UCLA PSPL has developed an electrohydrodynamics computational model (PSPL-EHD) to simulate electrospray development in the Extraction Region [8]. Droplet break-up occurs in the Transition Region, forming a multi-species plume which is no longer perfectly axisymmetric. In the Interaction Region, high-magnitude Coulombic interactions expand the plume until such interactions no longer dominate droplet dynamics, from which point forward we define the Plume Region. This publication focuses on the Interaction Region, in which a nearly co-linear set of multi-species droplets expands into a plume. The effects of droplet breakup in the Transition Region are represented by applying a spatial perturbation to a multi-species droplet population entering the Interaction Region.

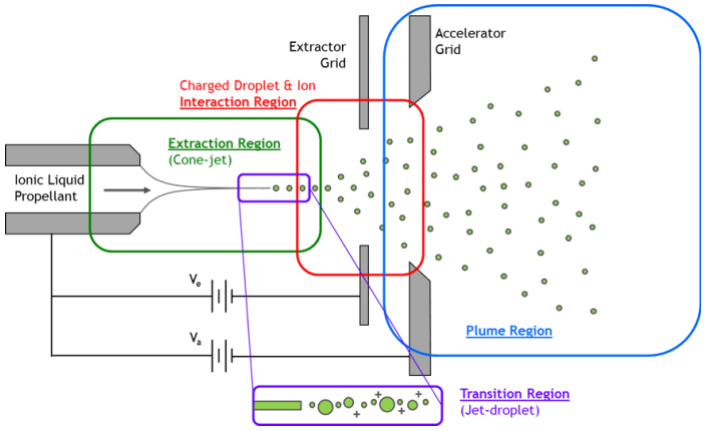

Figure 1: Discretization of the computational domain, reproduced courtesy of Wirz, *et al.* [2].

Electrosprays operating in the steady cone-jet mode have narrow, axisymmetric conical menisci and jets, yet produce wide plumes with diverse droplet populations [9], [10], [11], [12], [13]. Experimental plume profile measurements taken in the Plume Region feature large, lower-specific-charge droplets near the axis of emission and small, higher-specific-charge particles (droplets, ionic clusters, and/or single ions) at wider plume angles [ANI IEPC]. Several mechanisms which yield inhomogeneous droplet populations have been identified in both the Extraction and Transition Regions. Minute satellite droplets have been observed to be emitted between larger primary droplets using high speed videography [14], [10], and retarding potential analyzer and time-of-flight measurements [12]. Additionally, electric field-induced ion emission can occur from the fluid meniscus when the surface electric field magnitude surpasses a fluid-dependent threshold value on the order of $E \sim 1$ V/nm [15], [16]. Electric field strength on the meniscus surface is maximized at the cone apex, or "neck" of the cone-jet; however, ions may also be field emitted from the tip of the jet should the surface electric field strength there reach the threshold value [15], [17]. Fluids must be involatile enough to support cone-jet mode operation in vacuum and have sufficient conductivity to sustain surface electric fields of the threshold magnitude in order to field-emit ions from the meniscus.

Droplet breakup in the Transition Region can also contribute to inhomogeneity in the electrosprayed droplet population. Emitted droplets can field-emit ions if their surface electric field magnitude exceeds the fluid-dependent threshold ($E \sim 1$ V/nm) [15]. Droplet surface charge decreases following ion emission, thus decreasing the electric field strength at the surface of the droplet. Additionally, the imposed electric field on the droplets decreases rapidly downstream from emission. Due to the steep decrease in electric field magnitude at the droplet surface as the droplet moves downstream and emits ions, droplets can release only a small percentage of their total charge by ion field emission (estimated in the literature to be less than 10% of the total charge of the droplet) [15], [16].

An additional droplet breakup mechanism is Coulombic fission, or Coulombic explosion [11], [18]. The Rayleigh limit:

$$q_R = \pi\sqrt{8\gamma\epsilon_0 d_d^3}\,, \tag{1}$$

where γ is surface tension, d_d is droplet diameter, and ϵ_0 is the permittivity of free space, is the ideal maximum charge limit on a spherical droplet outside any electric field [19]. Electrospray droplets have been reported to fission with charges as low as 60% of the Rayleigh limit [20], [21], [22]. Such early-onset fissions may occur because electrospray droplets are removed from the ideal state for which the Rayleigh charge limit is defined; they are influenced by external electric fields and Coulombic interactions and have been optically observed to be non-spherical. Fissions have been observed to yield a wide variety of progeny droplets, from a few large daughter droplets with properties similar to the parents to fine sprays of many high-specific-charge droplets and ionic clusters [23]. Coulombic fissions have also been observed to be suppressed by electric field-driven ion emission from droplet surfaces [15]. The time required for ion emission is shorter than that of a Coulombic fission, causing droplets to preferentially field-emit ions.

III. Approach

The UCLA PSPL has developed an Interaction Model to simulate droplet dynamics in the Interaction Region, in which droplets are perturbed from a nearly co-linear state into a plume. The simulation domain begins directly following droplet emission and utilizes electric fields simulated using COMSOL Multiphysics software, given an applied voltage and electrode geometry. Droplet properties (mass, charge, radius, and instantaneous 3-D position, velocity, and acceleration) are user-defined or selected from experimental data. The model treats each droplet as a point charge subject to an applied electric field, as well as Coulombic, drag and gravitational forces, rationalized from the literature [24], [25]:

$$F_d = \sum_{i=0}^{N-1} k\frac{q_d q_i}{r_{d,i}^2} + q_d E + \frac{\pi r_d^2 \rho C_D (U - v_d)^2}{2} + g m_d\,, \tag{2}$$

where q is charge, m is mass, r is radius, $k = 8.99 \times 10^9$ N·m2/C2 is the Coulomb constant, E is electric field strength, ρ is density, C_D is the coefficient of drag, U is the velocity of the fluid medium (0 m/s in vacuum), v is droplet velocity, g is the gravitational constant, and N is the total number of droplets. Future work will incorporate image charge forces near the emitter and any electrodes. The forces described in Eq. 2 are depicted graphically in Figure 3.

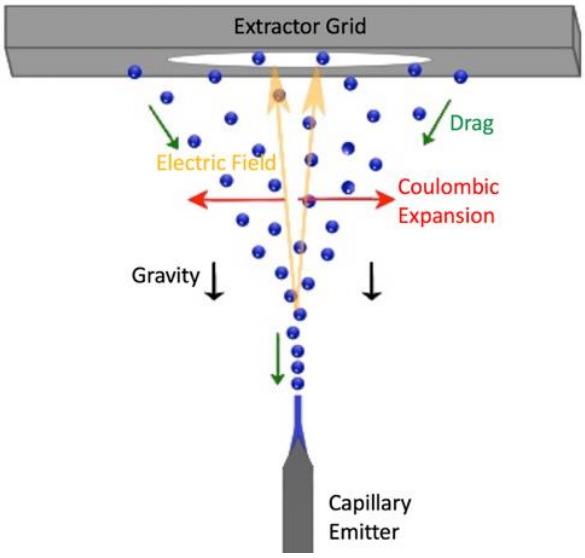

Figure 2: Coulombic, electric field, gravitational, and drag forces act on droplets in the plume.

A key parameter in modeling electrospray plume droplet dynamics is the computational timestep. Oversized timesteps allow droplets to pass one another without interacting Coulombically and could therefore corrupt simulated plume structures [26]. The Interaction Model employs an adaptive time-stepping mechanism to accurately capture Coulombic interactions. In each step, the model calculates the minimum separation distance between any two droplets $\left(r_{ij_{min}}\right)$ and the maximum velocity of any droplet (v_{max}) and defines a timestep,

$$\Delta t = \gamma_1 \frac{r_{ij_{min}}}{v_{max}}\,, \tag{3}$$

where $\gamma_1 \ll 1$ is a user-specified constant. The adapted timestep is then used to calculate the acceleration, velocity, and position of each particle using the force calculated in Eq. 2. Should the timestep, Δt, be insufficiently small to capture droplet dynamics (*i.e.* there exists some droplet which is highly accelerated such that it travels $\Delta x > \gamma_1 r_{ij}$, where r_{ij} is the distance to any other droplet), then the timestep is redefined:

$$\Delta t = \gamma_2 \frac{r_{ij_{min}}}{v_{max}}\,, \tag{4}$$

for $\gamma_2 < \gamma_1$ until Δt becomes sufficiently small. Sensitivity analyses are used to determine values for γ_1 that are computationally efficient without compromising model precision.

IV. Results

High-speed videography of ethanol electrosprays from the UCLA Atmospheric Pressure Electrospray Experiment (APEX) suggests that droplets that have a negative velocity gradient cluster in a "traffic jam," resulting in plume expansion [4], [27]. The theory of "traffic-jam-induced expansion" can be tested using the Interaction Model to compare the responses of two sets of droplets – one with constant droplet velocities and the other with dissimilar velocities – to the initial displacement of one droplet. The results of these simulations are depicted in Figure 4. In both cases, three identical ethanol droplets are evenly distributed over a distance $\Delta z = 0.1$ μm and the middle droplet is laterally displaced from the others by $\Delta x = 10$ fm $\ll \Delta z$. To isolate the droplet dynamics to only initial droplet motion and Coulombic interactions, gravity and drag are neglected and there is no imposed electric field. In case (a), in which the droplets have the same velocity ($v = 1$ m/s), droplets maintain their axial separation and are only slightly perturbed laterally via Coulombic interactions. However, in case (b), the droplet velocities increase front-to-back ($v_1 = 1$ m/s,

$v_2 = 2$ m/s, $v_3 = 3$ m/s), causing the droplets to cluster (a "traffic jam") and have Coulombic interactions of greater magnitude. The "traffic jam," coupled with the initial lateral offset of the middle droplet, causes all three droplets to be laterally displaced. These simulations demonstrate that collections of droplets with a negative velocity gradient in the downstream direction can expand considerably in response to perturbations too minute to have a significant expansion effect on constant-velocity droplets. A strictly positive velocity gradient would not cause droplets to cluster and thus not have the same effect. Therefore, our previous observation that negative velocity gradients between droplets can enhance plume expansion is corroborated by these simulations.

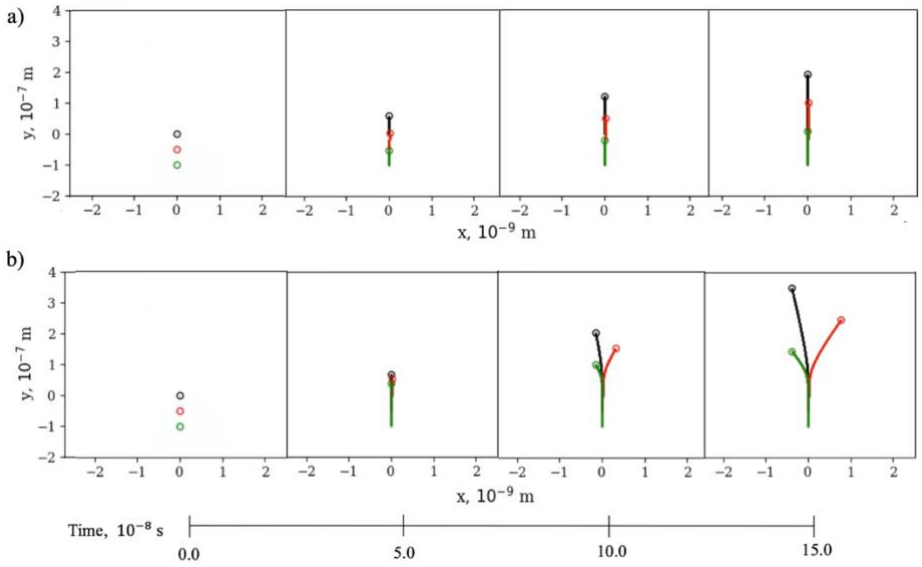

Figure 3: The middle droplet is initially displaced to the right by Δx = 10 fm in both cases. Droplets in case (a), moving at the same velocity v = 1 m/s, are radially displaced less by this initial perturbation than droplets in case (b), which have initial velocities v_1 = 1 m/s, v_2 = 2 m/s, v_3 = 3 m/s from front to back.

The Interaction Model can also examine interactions within experimental droplet populations and simulate resulting plume profiles. To demonstrate this ability, we utilize a droplet population previously electrosprayed over a 3.17 mm gap between electrodes with a 1950 V potential difference [9]. We define three discrete droplet species (*S*mall, *M*edium, and *L*arge → *S*, *M*, and *L*) from the observed droplet population for the case with beam current $I_B = 92$ nA (Table 1). Droplets are emitted one at a time per a user-designated discrete probability distribution. Following each droplet emission, a non-emission interval passes prior to the next droplet emission. The length of this interval is scaled based on droplet mass, and therefore species, in order to satisfy the experimental mass flow rate criteria, $\dot{m} = 14.4\,\mu g/s$. Per this flowrate requirement, the interval following a droplet of each species (denoted via subscript) is as follows:

$$t_S = \frac{m_S}{\dot{m}} = 2.79 \times 10^{-9}\ \text{s}\ ,\ \ t_M = \left(\frac{m_M}{m_S}\right) t_S = 3.38 t_S\ \ , t_H = \left(\frac{m_H}{m_S}\right) t_S = 15.6 t_s\ . \tag{5}$$

All simulated droplets are emitted with a velocity matching that of the jet into an electric field simulated in COMSOL Multiphysics based on the experimental emitter geometry [9]. The droplets are then electrostatically accelerated to different velocities based on their specific charges. We define a lateral sinusoidal perturbation to have period,

$$T_P = \alpha t_S\,, \tag{6}$$

where α is a scalable constant, so that the perturbation period can be scaled in relation to the time to emit a small droplet.

Defining dimensionless time,

$$\tau = \frac{2\pi t}{T_P} \,, \tag{7}$$

where t is current time in the simulation, we express the time-dependent lateral droplet emission coordinate as set by the sinusoidal perturbation:

$$x = \Delta x \sin(\tau) \,, \tag{8}$$

where the perturbation amplitude Δx is smaller than any droplet radius r_d so the perturbation may represent the effect of droplet break-up phenomena in the Transition Region, such as ion emission. Sinusoidal perturbations following the emission of small satellite droplets between larger primary droplets are photographically documented in the literature [14].

Table 1: Properties of 3 discrete droplet species based on an I_B = 92 nA beam current population [9].

Species	d [μm]	q [C]	m [kg]	q/m [C/kg]
[***S***]mall	0.4	8.04e-16	4.02e-17	20
[***M***]edium	0.6	1.36e-15	1.36e-16	10
[***L***]arge	1.0	3.14e-15	6.28e-16	5

To study the effects of droplet inhomogeneity and resulting velocity differences on plume expansion, we simulate and compare two plumes comprised of three discrete droplet species (Table 1) emitted with a sinusoidally perturbed lateral position (Eq. 2). In case (a), the droplets are evenly distributed between *L*, *M*, and *S* species. In case (b), there are 80% L, 10% M, and 10% S droplets. In both simulations, $\alpha = 1$ such that the perturbation period is equivalent to the non-emission interval following a Small droplet emission (Eq. 19). In addition, $\Delta x = 1$ nm for both cases, so the perturbation amplitude is smaller than any droplet radius and may therefore represent break-up phenomena which yield progeny significantly smaller than initially emitted droplets. Results for both plumes after $t = 2$ μs of simulated time are displayed in Figure 4. Plume evolution is demonstrated via cumulative mass profiles, cumulative charge profiles, and cumulative species frequency plume profiles (Figure 5 for the uniform species distribution plume and Figure 6 for the *L* - species dominated plume) for various distances from emission. Distance from emission is expressesed as a percentage of the emitter-extraction separation distance (*z*). In addition, each set of profiles in Figure 5 and Figure 6 is labelled with a value *n*, the percentage of total emitted droplets included in the profile. Note that near-emitter profiles include a higher percentage of emitted droplets than those further downstream because these simulation capture plumes from start-up emission conditions, so not all droplets have passed through all measurement planes. The location of each plume profile measurement plane displayed in Figure 5 and Figure 6 is labeled on the axis of Figure 4.

In both simulations, smaller droplets with higher specific charge are electrostatically accelerated to higher velocities than larger, lower specific charge droplets. The resulting "traffic jams" Coulombically repel smaller droplets to wide plume angles, whereas larger droplets are less displaced from the axis of emission. These observations are phenomenologically compatible with droplet dynamics observed using high-speed videography in the UCLA PSPL [28], [4] and with experimental plume profile results from which the droplet modes were selected [9].

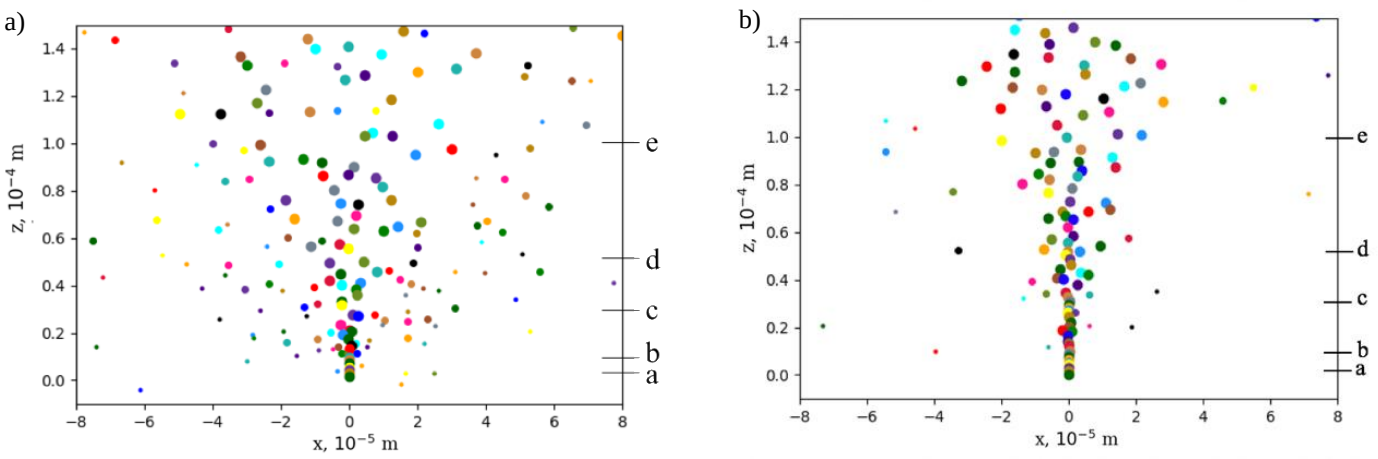

Figure 4: Simulated plume evolution for a) a plume with a uniform droplet species distribution between *L*, *M*, and *S*-species and b) a plume with 80% *L*-species, 10% *M*-species, and 10% *S*-species droplets.

In the case of the uniform species distribution plume, the large populations of *S*- and *M*-species droplets cause frequent traffic jams which significantly expand the plume. These frequent traffic jams allow several *S*-species droplets to reach plume angles of $\theta \geq 20°$ by only $z = 0.095$ % of the emitter-to-extractor distance dowstream of emission (Figure 5a). In the case of the *L*-species dominate plume, however, there are fewer small droplets to cause traffic jams, so the plume is narrower as a result. By $z = 0.095$ % downstream from emission, most *S*-species droplets occupy plume angles $\theta \leq 10°$ (Figure 6a). While both plumes expand rapidly following emission ($z \leq 0.5$ mm in Fig. 5), their angular plume profiles appear to narrow further downstream ($z = 1$ mm in Fig. 5). This behavior can be understood in the context of the regional discretization of the electorspray previously published by the UCLA PSPL. In the Interaction Region, droplets are densely packed and undergo large-magnitude Coulombic interactions which expand the plume in response to perturbations introduced in the Transition and Extraction Regions. The separation radii between droplets is increased as a consequence of these interactions, thus decreasing the magnitude of future Coulombic interactions between droplets. As a result of the diminishing influence of Coulombic interactions, droplet trajectories become increasingly electrostatically-dominated as droplets move from the Interaction Region to the Plume Region. Therefore, plume profiles should be expected to narrow as droplets move downstream from the Interaction to Plume Region because Coulombic interactions, the primary means of plume expansion, are no longer dominant over the applied electric field. The experimental plume profile data from which the 3 droplet modes were selected features *L*-species droplets at plume angle $\theta \sim 6°$, *M*-species droplets at to $\theta \sim 16°$, and *S*-species droplets reaching angles of $\theta \sim 28°$ [9]. This experimental data was measured significantly downstream of the extractor grid, with the understanding that the plume structure will not have changed substantially since passing the extractor grid. While the experimental plume is narrower than both given simulation results, the simulations represent the plume only a fraction of the distance to the extractor grid ($z = 3.2\%$) (Figure 5d and Figure 6d). Simulated plumes can be understood to narrow significantly downstream under the influence of applied electric fields as droplets pass from the Interaction to Plume Region. Additionally, the plume profiles at $z = 1.6\%$ (Figure 5d and Figure 6d) contain a larger portion of emissted droplet than the profiles at $z = 3.2\%$ (Figure 5e and Figure 6e). Therefore, it is possible that the widest droplets measured at $z = 1.6\%$ are not present in the $z = 3.2\%$ cumulative species frequency profiles. In this case, the latter $z = 3.2\%$ would appear wider after more simulation time when such wide-angle droplets have traveled further downstream.

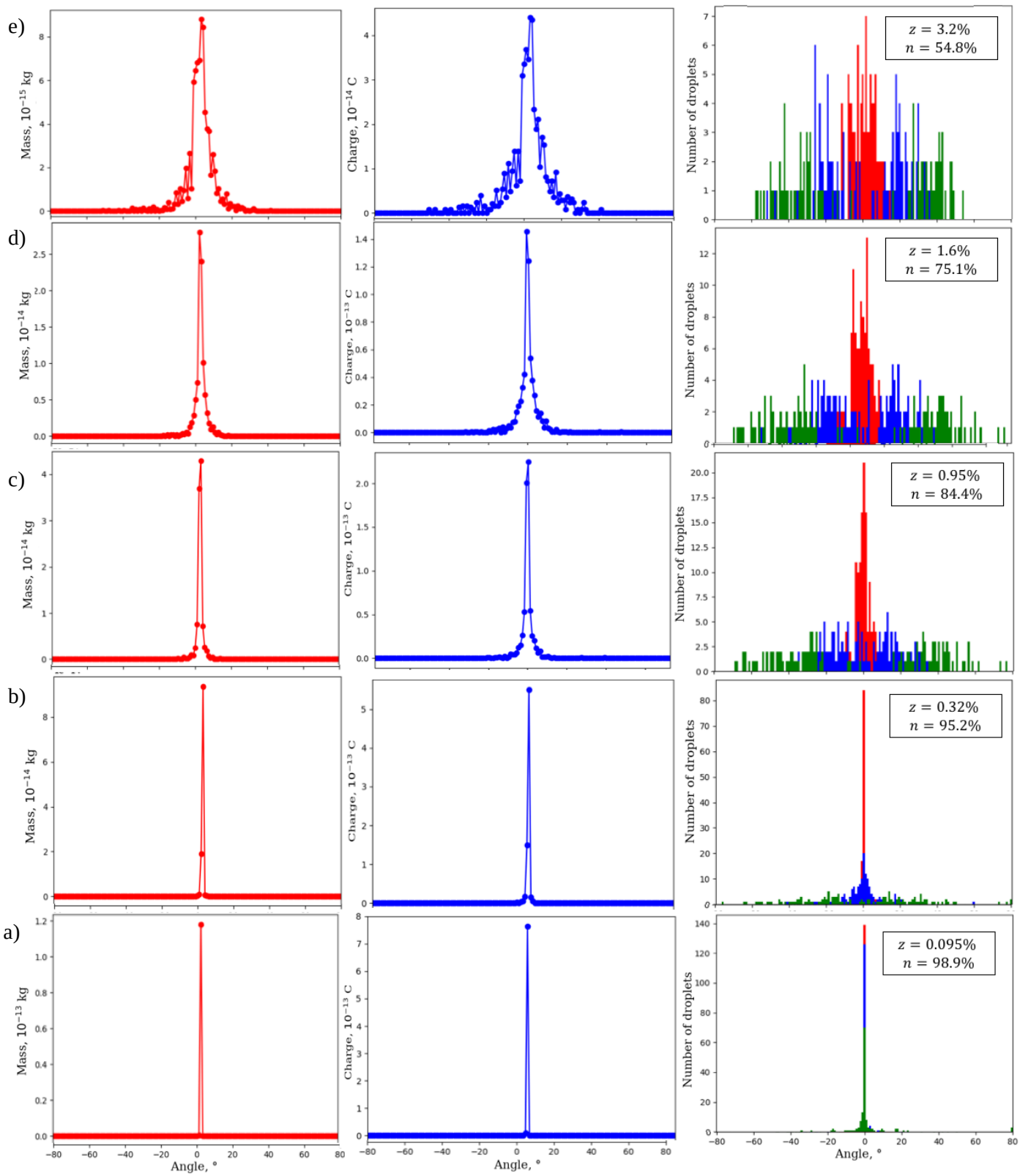

Figure 5: Cumulative mass profiles, charge profiles, and species frequency profiles are given at various distances from the emitter, a) - e), for a plume with a uniform droplet distribution between the three species. In the frequency profiles, red represents H-species droplets, blue is for M-species, and green marks S-species.

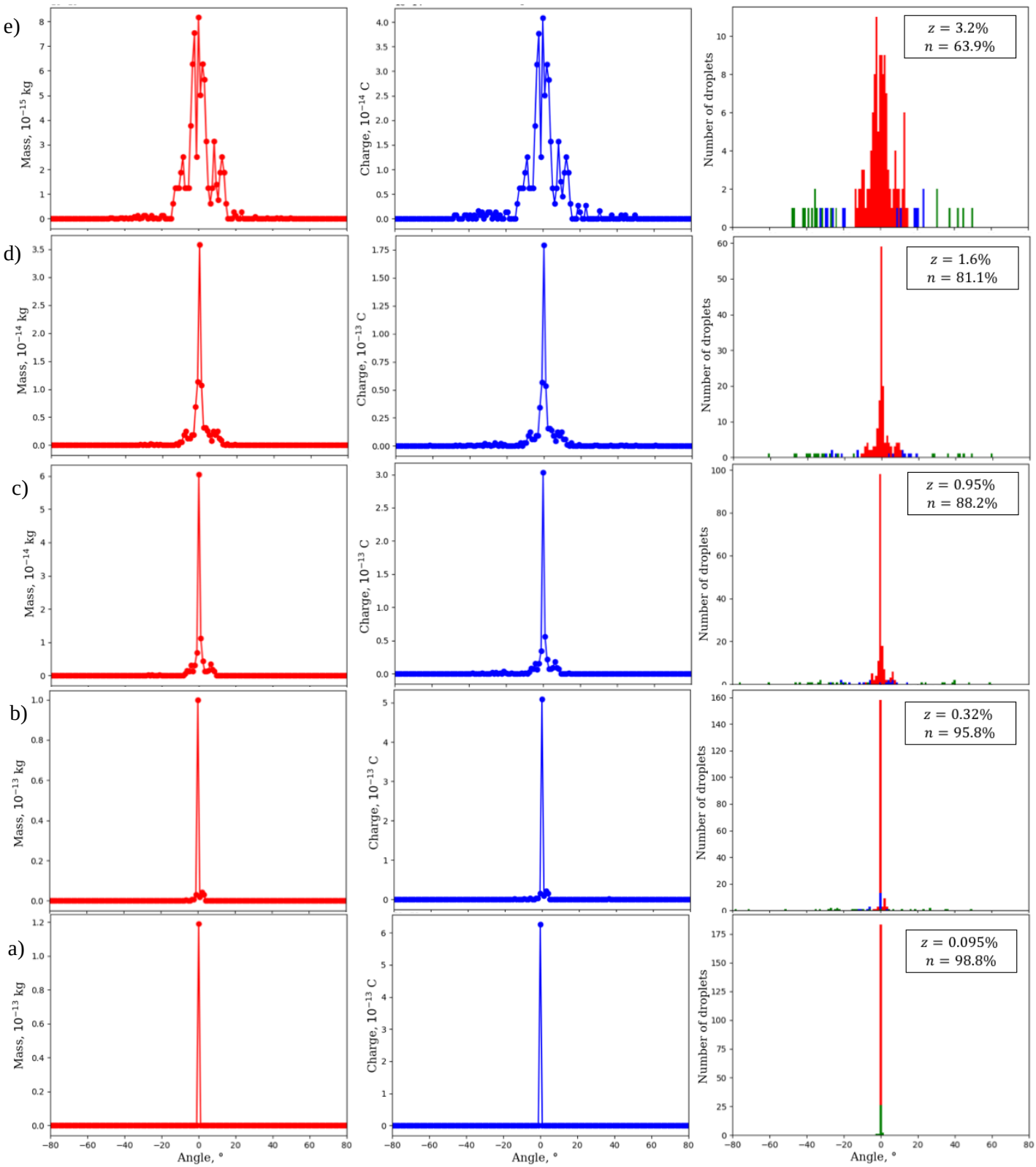

Figure 6: Cumulative mass profiles, charge profiles, and species frequency profiles at various distances from the emitter, a) - e), for a plume with 80% L-species, 10% M-species, and 10% S-species droplets. In the frequency profiles, red represents H-species droplets, blue is for M-species, and green marks S-species.

Differences in cumulative mass and charge profiles are also evident between the two simulated plumes. The evolution of these two plumes are directly compared in Figure 7, in which 2 standard deviations of the cumulative charge and mass plume profile widths (plume angles encompassing 95% of total mass or charge) are plotted as a function of percent distance to extractor grids (z). The cumulative mass and charge profile expand more quickly in the uniform-species distribution case than in the L-species dominated case; this difference in near-emitter plume width is most noticeable at $z = 0.16\%$. Further downstream ($z \geq 0.16\%$), the evolution of the two plumes becomes more similar, perhaps suggesting that droplet trajectories in the plume are becoming increasingly electrostatically dominated as they exit the Interaction Region. Additional analyses of the forces acting on each droplet as a function of percent distance to extractor grids will serve to demarcate such a transition from Interaction to Plume Region; these analyses are dedicated as future work. The sensitivity of the developing plume shape to the initial droplet population is evident in the plume evolution comparison provided in Figure 7.

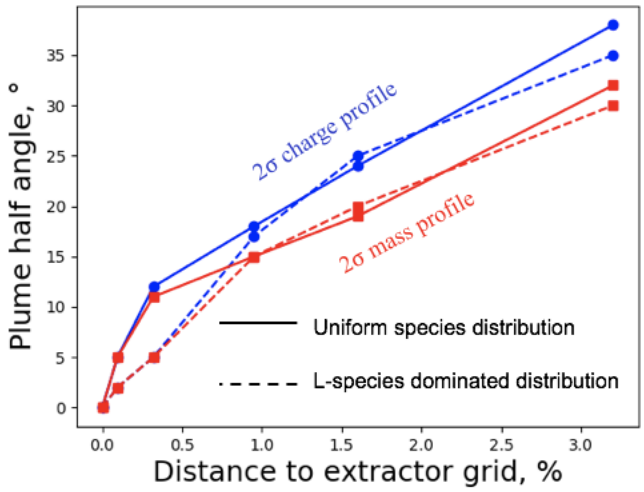

Figure 7: The plume angle which contains 95% of the quantity of interest (2 standard deviations of the plume profile width) is plotted as a function of percent distance to extractor grid (z) for the cumulative charge (blue) and cumulative mass (red) profiles given for the uniform species distribution plume (Figure 5, represented with solid lines) and the *L*-species dominated plume (Figure 6, shown with dotted lines).

V. Conclusion

The Interaction Model developed by the UCLA PSPL has confirmed that negative velocity gradients of emitted droplets can cause significant plume expansion in response to Coulombic "traffic jams." Inhomogeneous droplet velocity distributions can arise from the electrostatic acceleration of inhomogeneous droplet populations, which are created through a variety of phenomena in the Extraction and Transition Regions (such as satellite droplet emission, electric-field-induced ion emission from the fluid meniscus and droplets, and Coulombic fissions). While the Interaction Model does not currently simulate these complex breakup mechanisms, the inclusion of these phenomena is designated as the future work of this effort. Simulation results display angular droplet segregation by specific charge, phenomenologically replicating experimental observations. In addition, simulated animations of plume evolution and resulting plume profiles emphasize the sensitivity of plume to the initial modal distribution

of the droplet population. Improved understandings of the emitted droplet population and droplet breakup mechanisms will allow for the advancement of the Interaction Model in the future.

VI. Acknowledgements

The authors would like to thank John Ziemer, Colleen Marrese-Reading, and Alejandro López Ortega from NASA JPL, Nathaniel Demmons from Busek, Manuel Gamero-Castaño from the University of California, Irvine, and Mihir Sharma from UCLA for their insightful discussions. This work was supported by a National Defense Science and Engineering Fellowship.

References

[1] J. Ziemer, Mar, A. Romero-Wolf, C. Cutler, S. Javidnia, T. Li, I. Li, G. Franklin and P. Barela, "Colloid microthruster flight performance results from space technology 7 disturbance reduction system.," in *International Electric Propulsion Conference*, Atlanta, 2017.

[2] R. E. Wirz, A. L. Collins, A. Thuppul, P. L. Wright, N. M. Uchizono, H. Huh and M. J. Davis, "Electrospray Thruster Performance and Lifetime Investigation for the LISA Mission," in *AIAA Propulsion and Energy Forum and Exposition*, Indianapolis, 2019.

[3] R. E. Wirz, A. L. Collins, Z. Chen, C. Huerta, G. Li, S. A. Samples, A. Thuppul, P. L. Wright, N. M. Uchizono, H. Huh, M. J. Davis and A. Ottaviano, "Electric Propulsion Activities at the UCLA Plasma & Space Propulsion Laboratory," in *International Eletric Propulsion Conference IEPC-2019-547*, Vienna, Austria, 2019.

[4] A. Thuppul, P. L. Wright and R. E. Wirz, "Lifetime Considerations and Estimation for Electrospray Thrusters," in *AIAA Joint Propulsion Conference*, Cincinnati, 2018.

[5] A. L. Collins, A. Thuppul, P. L. Wright, N. M. Uchizono, H. Huh, M. J. Davis, J. K. Ziemer, N. R. Demmons and R. E. Wirz, "Assessment of Grid Impingement for Electrospray Thruster Lifetime," in *International Electric Propulsion Conference, IEPC-2019-213*, Austria, 2019.

[6] N. M. Uchizono, A. L. Collins, A. Thuppul, P. L. Wright, D. Q. Eckhardt, J. K. Ziemer and R. E. Wirz, "Electrospray Transient Emission Behavior and Spatial Stability," in *International Electric Propulsion Conference, IEPC-2019-368*, Vienna, Austria, 2019.

[7] A. Thuppul, A. L. Collins, P. L. Wright, N. M. Uchizono and R. E. Wirz, "Spatially-Resolved Mass Flux and Current Measurements for Electrospray Plumes," in *International Electric Propulsion Conference, IEPC-2019-571*, Vienna, Austria, 2019.

[8] H. Huh and R. E. Wirz, "Numerical Simulation of Electrospray Extraction for Highly Conductive Propellants," in *International Electric Propulsion Conference, IEPC-2019-565*, Austria, 2019.

[9] M. Gamero-Castaño, "The Structure of Electrospray Beams in Vacuum," *Journal of Fluid Mechanics*, vol. 604, pp. 339-368. doi:10.1017/s0022112008001316, 2008.

[10] W. Deng and A. Gomez, "Influence of Space Charge on the Scale-up of Multiplexed Electrosprays," *Journal of Aerosol Science*, vol. 38, no. 10, pp. 1062-1078. doi:10.1016/j.jaerosci.2007.08.005, 2007.

[11] A. Gomez and K. Tang, "Charge and Fission of Droplets in Electrostatic Sprays," *Physics of Fluids*, vol. 6, no. 1, pp. 404-414. doi:10.1063/1.868037., 1994.

[12] M. Gamero-Castaño, "Characterization of the electrosprays of 1-ethyl-3-methylimidazolium bis(trifluoromethylsulfonyl) imide in vacuum," *Physics of Fluids*, vol. 20, no. 3, p. 032103, 2008.

[13] J. Fernández de la Mora, "The effect of charge emission from electrified liquid cones," *Journal of Fluid Mechanics*, vol. 243, pp. 561-574, 1992.

[14] K. Tang and A. Gomez, "On the Structure of an Electrostatic Spray of Monodisperse Droplets," *Physics of Fluids*, vol. 6, no. 7, pp. 2317-2332, 1994.

[15] M. Gamero-Castaño and J. Fernández De La Mora, "Direct Measurement of Ion Evaporation Kinetics from Electrified Liquid Surfaces," *The Journal of Chemical Physics*, vol. 113, no. 2, pp. 815-832, 2000.

[16] M. Gamero-Castaño, "Electric-Field-Induced Ion Evaporation from Dielectric Liquid," *Physical Reveiw Letters*, vol. 89, no. 14, p. 147602, 2002.

[17] W. D. Luedtke, U. Landman, Y. H. Chio, D. Levandier, R. Dressler, S. Sok and M. Gordon, "Nanojets, Electrospray, and Ion Field Evaporation: Molecular Dynamics Simulations and Laboratory Experiments," *The Journal of Physical Chemistry A*, vol. 112, no. 40, pp. 9628-9649. doi:10.1021/jp804585y, 2008.

[18] K.-Y. Li, T. Haohua and A. K. Ray, "Charge Limits on Droplets during Evaporation," *Langmuir*, vol. 21, no. 9, pp. 3786-3794. doi:10.1021/la047973n, 2005.

[19] L. R. F.R.S., "On the equilibrium of liquid conducting masses charged with electricity," *The London, Edinburgh, and Dublin Philosophical Magazine and Journal of Science*, vol. 5, no. 14, pp. 184-186, 1882.

[20] D. C. Taflin, T. L. Ward and E. J. Davis, "Electrified Droplet Fission and the Rayleigh Limit," *Langmuir*, vol. 5, no. 2, pp. 376-384. doi:10.1021/la00086a016, 1989.

[21] K. Tang and R. D. Smith, "Physical/Chemical Separations in the Break-up of Highly Charged Droplets from Electrosprays," *Journal of the American Society for Mass Spectrometry*, vol. 12, no. 3, pp. 343-347. doi:10.1016/s1044-0305(01)00222-7, 2001.

[22] E. Davis and a. M. Bridges, "The Rayleigh Limit of Charge Revisited: Light Scattering from Exploding Droplets," *Journal of Aerosol Science*, vol. 25, no. 6, pp. 1179-1199. doi:10.1016/0021-8502(94)90208-9, 1994.

[23] J. Fernandez de la Mora, "On the Outcome of the Coulombic Fission of a Charged Isolated Drop," *Journal of Colloid and Interface Science*, vol. 178, no. 1, pp. 209-218, 1996.

[24] A. Gañán-Calvo, J. Lasheras, J. Davila and A. Barrero, "The Electrostatic Spray Emitted from an Electrified Conical Meniscus," *Journal of Aerosol Science*, vol. 25, no. 6, pp. 1121-1141. doi:10.1016/0021-8502(94)90205-4., 1994.

[25] J. Rosell-Llompart, J. Grifoll and I. G. Loscertales, "Electrosrpays in the cone-jet mode: From Taylor cone formation to spray development," *Jounral of Aerosol Science*, vol. 125, pp. 2-31, 2018.

[26] J. Grifoll and J. Rossell-Llompart, "Efficient Lagrangian Simulation of Electrospray Droplets Dynamics.," *Journal of Aerosol Science*, vol. 47, pp. 78-93, 2012.

[27] P. Wright, A. Thuppul and R. Wirz, "Life-Limiting Emission Modes for Electrospray Thrusters," in *Joint Propulsion Conference, AIAA 2018-4726*, Cincinnati, 2018.

[28] A. Thuppul, P. Wright and R. Wirz, "Lifetime Considerations and Estimation for Electrospray Thrusters," in *2018 AIAA Joint Propulsion Conference*, 2018.